Published April 22, 2016

Mineralogical Transformations and Soil Development in Shale across a Latitudinal Climosequence

Ashlee L. Dere*
Dep. of Geography and Geology
Univ. of Nebraska–Omaha
6001 Dodge Street
Omaha, NE 68182

Timothy S. White
Earth and Environmental Systems Institute
The Pennsylvania State Univ.
University Park, PA, 16802

Richard H. April
Dep. of Geology
Colgate Univ.
336 Ho Science Center
Hamilton, NY 13346

Susan L. Brantley
Earth and Environmental Systems Institute
The Pennsylvania State Univ.
University Park, PA 16802
and
Department of Geosciences
The Pennsylvania State Univ.
University Park, PA 16802

To investigate factors controlling soil formation, we established a climosequence as part of the Susquehanna-Shale Hills Critical Zone Observatory (SSHCZO) in central Pennsylvania, USA. Sites were located on organic matter-poor, iron-rich Silurian-aged shale in Wales, Pennsylvania, Virginia, Tennessee, Alabama, and Puerto Rico, although this last site is underlain by a younger shale. Across the climosequence, mean annual temperature (MAT) increases from 7 to 24°C and mean annual precipitation (MAP) ranges from 100 to 250 cm. Variations in soil characteristics along the climosequence, including depth, morphology, particle-size distribution, geochemistry, and bulk and clay mineralogy, were characterized to investigate the role of climate in controlling mineral transformations and soil formation. Overall, soil horizonation, depth, clay content, and chemical depletion increase with increasing temperature and precipitation, consistent with enhanced soil development and weathering processes in warmer and wetter locations. Secondary minerals are present at higher concentrations at the warmest sites of the climosequence; kaolinite increases from <5% at northern sites in Wales and Pennsylvania to 30% in Puerto Rico. The deepest observed weathering reaction is plagioclase feldspar dissolution followed by the transformation of chlorite and illite to vermiculite and hydroxy-interlayered vermiculite. Plagioclase, although constituting <12% of the initial shale mineralogy, may be the profile initiating reaction that begins shale bedrock transformation to weathered regolith. Weathering of the more abundant chlorite and illite minerals (~70% of initial mineralogy), however, are more likely controlling regolith thickness. Climate appears to play a central role in driving soil formation and mineral weathering reactions across the climosequence.

Abbreviations: CZ, critical zone; HIV, hydroxy-interlayered vermiculite; ICP-AES, inductively coupled plasma atomic emission spectroscopy; LGM, last glacial maximum; MAP, mean annual precipitation; MAT, mean annual temperature; MCL, Materials Characterization Laboratory; SRT, soil residence time ; SSHCZO, Susquehanna-Shale Hills Critical Zone Observatory; XRD, x-ray diffraction.

Core Ideas

- **Detailed characterization of the morphology, geochemistry, and mineralogy of shale-derived soils across a climosequence documents enhanced weathering and soil development with increasingly warm and wet climates.**
- **The deepest weathering reaction observed in the regolith across the shale climosequence was plagioclase feldspar dissolution, which may be the profile initiating reaction that begins the transformation of shale bedrock to weathered regolith.**
- **The abundance of chlorite and its transformation to vermiculite and HIV are more likely controlling regolith thickness in these soils.**

Quantifying changes in the critical zone (CZ), especially soil development and function, is important for predicting the future of soils (NRC, 2001). The CZ extends from the top of the vegetation canopy to freshwater aquifers beneath Earth's surface and is the focus of most ecosystem processes that support terrestrial life (Brantley et al., 2007). Soil formation within the CZ involves complex coupling between physical, chemical, and biological processes that are not well quantified (Amundson, 2004). Efforts to predict how future changes in climate and land use will modify the CZ are ongoing and are important aspects of developing adaptation and management plans for human society (Banwart et al., 2011).

Supplemental material available online.
Open Access
Soil Sci. Soc. Am. J.
doi:10.2136/sssaj2015.05.0202
Received 26 May 2015.
Accepted 31 Dec. 2015.
*Corresponding Author (adere@unomaha.edu).

A state factor approach is commonly used to investigate a soil property or function as the result of various environmental factors, including climate, biota, topography, parent material, and time (Dokuchaev, 1883; Jenny, 1941). Using environmental gradients to isolate the influence of one soil forming factor is a practical approach to solving the state factor equation (e.g., Runge 1973; Birkeland, 1999). Climate is of particular interest because it plays an important role in mineral weathering and soil formation whereby more intense weathering is associated with high temperatures and precipitation rates (White and Brantley, 1995). Water is necessary to facilitate mineral transformation reactions: water temperature in part controls the kinetics of the system such that weathering reactions occur more rapidly in the presence of warm rather than cool water (Kump et al., 2000). Furthermore, increasing temperature decreases the amount of water available for weathering by partitioning more precipitation to evapotranspiration rather than baseflow (Rasmussen et al., 2005).

Strong climate gradients are observed either across elevation or latitudinal changes. Elevation gradients encompass a range of precipitation and temperature across short distances and record climate effects on soil development and weathering (e.g., Koch et al., 1995; Dahlgren et al., 1997; Bockheim et al., 2000; Egli et al., 2003; Stiles et al., 2003; Goodfellow et al., 2014). Similarly, soil profiles observed across latitudinal gradients (Muhs et al., 2001; Williams et al., 2010) or at a variety of latitudes (Rasmussen et al., 2011) show correlations of climate to weathering rates and mineral transformations.

In landscapes where physical erosion is low, studies at multiple spatial scales have demonstrated that precipitation and temperature strongly control chemical weathering rates and soil development when all other state factors are held constant (Strakhov, 1967; Ruhe, 1984; Chadwick et al., 2003; Dahlgren et al., 1997; Rasmussen et al., 2007; Williams et al., 2010; Goodfellow et al., 2014). The degree of soil development varies considerably with changes in climate, with thresholds observed in weathering processes and soil formation between water-limited systems and energy-limited systems (Dahlgren et al., 1997; Rasmussen et al., 2011; Goodfellow et al., 2014). Soil development indices correlated with climate include increased clay content (Dahlgren et al., 1997; Bockheim et al., 2000; Lybrand and Rasmussen, 2015), elemental losses and redistributions during pedogenesis (Muhs et al., 2001; Egli et al., 2003; Stiles et al., 2003; Chadwick et al., 2003) and mineral transformations from parent material to secondary clay minerals in soils (Dahlgren et al., 1997; Mirabella and Egli, 2003).

As weathering of residual bedrock proceeds, minerals in the parent material are transformed to clay minerals such as vermiculite, hydroxy-interlayered vermiculite (HIV), and kaolinite, and iron oxides (Wilson, 2004). Common weathering reactions in soils include the transformation of chlorite and illite to vermiculite, HIV, and interstratified clay minerals (April et al., 1986; Wilson, 1999). Some mineral weathering reactions, such as carbonate dissolution, pyrite oxidation or plagioclase feldspar dissolution, are described as profile initiating reactions that begin the process of disaggregating bedrock into regolith; weathering reactions such as clay dissolution, however, are likely more important in controlling the overall regolith thickness (Brantley et al., 2013). Indeed, studies on various lithologies have documented the deepest weathering reactions as carbonate dissolution (White et al., 2005; Williams et al., 2007; Jin et al., 2010), biotite oxidation (Buss et al., 2008; Behrens et al., 2015; Bazilevskaya et al., 2015), or plagioclase feldspar dissolution (Brantley and White, 2009; Behrens et al., 2015) but these minerals sometimes constitute a small fraction of the overall parent mineralogical composition.

An increasing number of quantitative weathering models are advancing our ability to predict weathering advancement and landscape evolution (e.g., Godderis et al., 2006; Lebedeva et al., 2007, 2010; Brantley et al., 2008; Minasny et al., 2008; Maher, 2010; Brantley and Lebedeva, 2011; Bazilevskaya et al., 2013, 2015) but field observations of soil thickness, geochemistry, and mineralogy are needed across a range of environmental gradients to validate these models (Behrens et al., 2015). In an effort to investigate soil formation as a function of climate, a climosequence of sites was established on residual shale parent material in the Northern Hemisphere. The climosequence encompasses mean annual temperature (MAT) of 7 to 24°C and mean annual precipitation (MAP) ranging from 100 to 250 cm. Parent material is dominantly Silurian organic matter-poor, iron-rich Rose Hill Formation shale across sites that are currently tectonically quiescent and at relatively low elevation (240–750 m). Previous research efforts across this climosequence focused on quantifying weathering rates as a function of climate, where we observed an exponential dependence of temperature and a linear dependence of precipitation on plagioclase weathering rates (Dere et al., 2013). The aim of this paper is to document mineralogical transformations and soil development across a climosequence of shale-derived soils to identify weathering reactions controlling soil thickness and development, and to further investigate the role of climate in controlling soil formation.

MATERIALS AND METHODS

Climosequence Locations

The climosequence spans 34° of latitude in the Northern Hemisphere and includes the following sites: Plynlimon, Wales, United Kingdom; Whipple Dam State Park and SSHCZO, Pennsylvania (PA), USA; Goshen National Wildlife Management Area, Virginia (VA), USA; Big Ridge State Park, Tennessee (TN), USA; Lake Guntersville State Park, Alabama (AL), USA; and Juncal, Puerto Rico (PR), USA (Fig. 1; Table 1). These sites were previously described in detail in Dere et al. (2013). Mean annual temperature and MAP vary across the climosequence, with the Wales and PR end member sites exhibiting the greatest difference in climate (Table 1). The majority of the sites are underlain by Silurian iron-rich, organic-poor Clinton Group shale. In PA and VA, the shale is part of the Rose Hill Formation (Gillette, 1947; Folk, 1960; Kozak, 1965) while shale formations in TN and AL are called the Rockwood and Red Mountain Formations, respectively (Finlayson, 1964; Sanford,

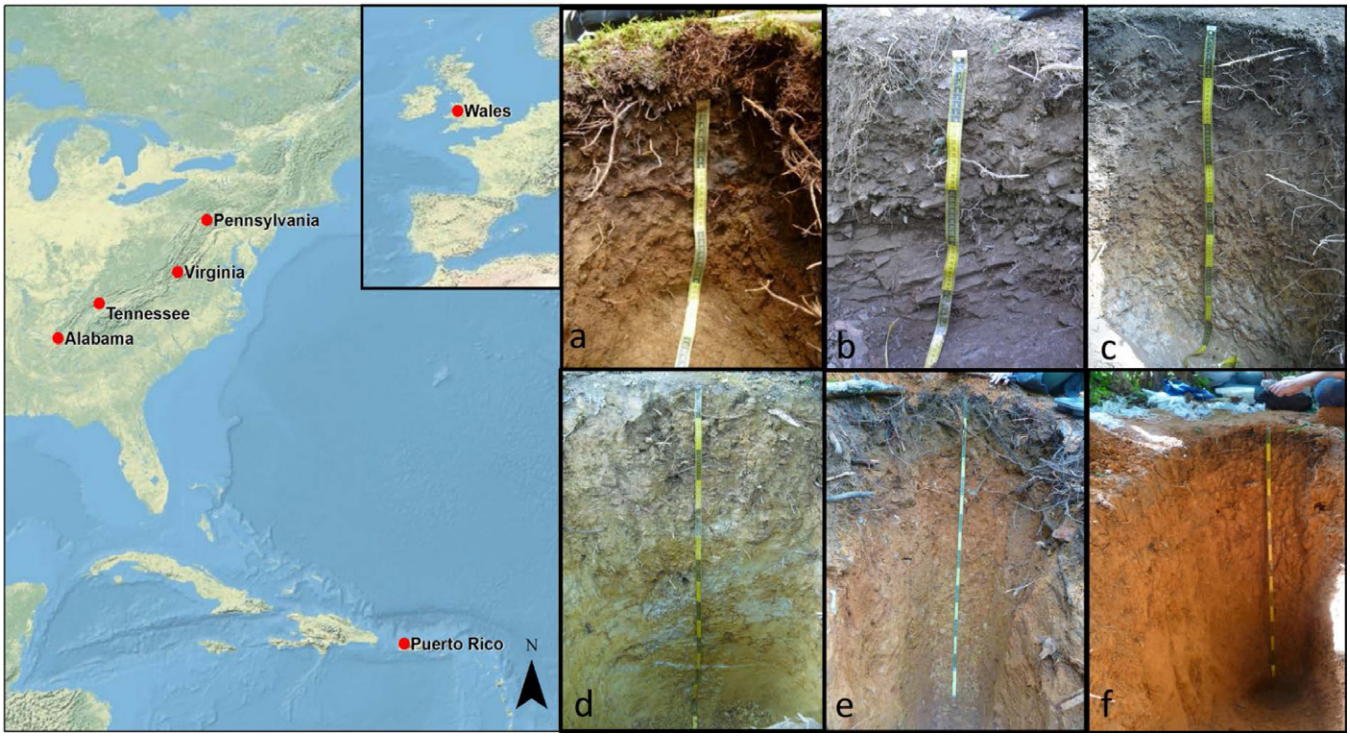

Fig. 1. Map of sampling sites in the shale climosequence and photographs of ridgetop soils from (a) Wales, (b) Pennsylvania, (c) Virginia, (d) Tennessee, (e) Alabama, and (f) Puerto Rico. Black and yellow intervals are each 10 cm.

1966). The shale in Wales is part of the Gwestyn Formation (British Geological Survey, 2005). Puerto Rico does not have Silurian shale therefore an Oligocene shale (Tobish and Turner, 1971) was sampled at this site. Residual soil profiles on ridgetop topographic positions were sampled at all sites to minimize any colluvial inputs (Taylor and Eggleton, 2001).

Vegetation varies across the climosequence, as would be expected across any climatic gradient. The Appalachian Mountains are dominated by mixed deciduous forests with coniferous vegetation most prominent in the northern study sites. The vegetation in Wales consists of spruce plantations on the slopes and moorland grasses in the upper reaches of the watershed. Puerto Rico has tropical species including banana (*Musa* sp.) and palm (*Arecaceae* sp.) trees. Although we attempted to sample sites undisturbed by humans, we recognize that the Appalachian Mountains have been deforested several times in the last 300 yr (Walter and Merritts, 2008). Puerto Rico was managed as a farm as recently as 40 yr ago and Wales is an active spruce plantation.

Aside from human disturbances, the greatest climatic disturbance over the soil residence time (SRT), or the time soils have been forming, at each site was the Last Glacial Maximum (LGM) where glaciers covered Wales and periglacial conditions persisted in PA until about 15 ka (Ciolkosz et al., 1986; Cadwell and Muller, 2004; Catt et al., 2006). Although periglacial features have been reported throughout much of the Appalachian Mountains (King et al., 1960; Clark and Ciolkosz, 1988; Gardner et al., 1991), we did not observe these features in the soil pits at sites other than central PA.

Soil and Rock Sampling

Soil samples were collected using a 5-cm diam. hand auger from the mineral soil surface to refusal or as deep as physically possible; in some profiles we were unable to manually auger to unweathered bedrock and therefore the weathering profile extends deeper than sampled. An auger was used to retrieve deep soil samples in TN, AL, and PR; at these sites, we augered from the soil surface to as deep as possible but then continued augering from the base of hand-dug soil pits to extend our augerable depth. The interface between the organic and mineral horizon was defined as 0 cm. Samples were collected approximately every 10 cm throughout the augerable profile and placed in a resealable plastic bag for storage. Soil pits were dug by hand up to 2 m deep and described (Soil Survey Staff, 1993). To maintain consistency with all samples in this study, we analyzed only augered soil samples even for those samples that were possible to retrieve from soil pits. Rock samples were obtained from outcrops near soil sampling sites or from the bottom of soil pits (see Dere et al. [2013] for locations). All samples were air-dried and homogenized before chemical and physical analyses.

Table 1. Locations and mean annual temperature (MAT) and precipitation (MAP) for each site in the climosequence.

Site	Latitude	Longitude	MAT	MAP
			°C	mm yr^{-1}
Wales	52.47360	-03.69292	7.98	2320
Pennsylvania	40.66552	-77.90495	10.1	1160
Virginia	37.92708	-79.54665	11.1	1180
Tennessee	36.27357	-83.91348	14.5	1210
Alabama	34.42292	-86.20667	16.5	1580
Puerto Rico	18.30083	-66.90668	23.0	2510

Soil and Rock Chemistry

Bedrock and bulk soil sample splits (including any rock fragments) were ground and passed through a 100-mesh sieve (<150 μm). In preparation for chemical analysis, 1 g of lithium metaborate was fused with 100 mg of ground sample at 950°C for 10 min followed by dissolution in 5% (v/v) nitric acid for 30 min (Medlin et al., 1969). The resulting solutions were analyzed for major elements by inductively coupled plasma atomic emission spectroscopy (ICP–AES; PerkinElmer Optima 5300DV ICP–AES, Waltham, MA). These analyses were performed at the Materials Characterization Laboratory (MCL) at Penn State University with an estimated analytical error of ±3% for each element.

Soil chemical profiles were interpreted using the dimensionless mass transfer coefficient:

$$\tau_{i,j} = \frac{C_{j,w}\, C_{i,p}}{C_{j,p}\, C_{i,w}} - 1 \qquad [1]$$

where τ represents the ratio of the concentration of an element of interest (C_j) normalized to an immobile element (C_i) in the weathered soil (w), and unweathered parent material (p; Brimhall and Dietrich, 1987; Anderson et al., 2002). A τ value of zero indicates an element has not changed from the initial parent composition, while a τ value greater than or less than zero indicates addition or depletion of an element relative, respectively, to the initial parent composition (Brimhall and Dietrich, 1987). The τ value is a useful way to compare changes in elemental composition from weathering processes, especially given the variations, albeit small, in initial parent composition between sites along the climosequence (Dere et al., 2013). Parent material was defined as the average of shale samples from local shale outcrops or rocks recovered from pits or boreholes. Across the climosequence, Zr was observed to be less mobile than Ti and was therefore chosen as the immobile element in Eq. [1]. In VA, however, Zr addition to the profile from denudation and incorporation of previously overlying sandstone precluded the use of Zr as the immobile element; instead, we used corrected Ti values to account for Ti mobility (Jin et al., 2010; Dere et al., 2013).

Soil Particle-Size Distribution

Soil particle-size distribution (wt %) was measured by first passing 15 g of soil through a 2-mm sieve to remove any rock fragments. Ten grams of the <2-mm fraction was then placed in a 250-mL centrifuge bottle and filled halfway with distilled water (Soil Survey Staff, 2004). Samples were sonified for 10 min then placed on a shaker table for 30 min before pouring the silt and clay suspension through a wetted 53-μm sieve and rinsing with approximately 500 mL of distilled water to separate the sand fraction (2 mm–53 μm) from the silt and clay fractions (Jackson, 1974; Soil Survey Staff, 2004). The rock and sand fractions were dried overnight at 105°C and weighed after cooling. The remaining silt and clay suspension was analyzed by laser diffraction using a Malvern Mastersizer "S" V. 2.19 (Malvern Instruments Ltd., Malvern, UK) at the MCL. This instrument has a size range of 0.05 to 900 μm and we used a wavelength of 633 nm, beam length of 2.4 cm and a particle density of 2.65 g cm^{-3}. Distilled water was used as the medium with a refractive index of 1.33 at 20°C; the refractive index of illite (1.54) was used for the solid phase, with an obscuration of ~15% (Buurman et al., 1997). The laser diffraction method measures the variation in light scattering intensity as a laser beam passes through a well dispersed sample, yielding a volume distribution of particle-sizes. Such an approach assumes that all particles are spheres, which is unrealistic for clay particles exhibiting platy structure. Thus, we defined the clay-sized fraction as particles < 8 μm based on previous work by Konert and Vandenberghe (1997) that compared the laser and pipette particle-size analysis methods. The percentage volume of silt and clay obtained by laser diffraction was converted to weight percentage by subtracting the sand fraction from the original mass of the sample (10 g) and dividing the remaining mass proportionally between the silt and clay fraction so the sum of all three size fractions (sand, silt, and clay) totaled 100%.

Quantitative Bulk Soil and Rock Mineralogy

Select soil and rock samples from sites across the climosequence were analyzed for mineralogy using X-ray diffraction (XRD). For quantitative XRD analysis, 1 g of ground sample (<150 μm) was combined with 0.25 g of corundum standard and micromilled with ethanol using a McCrone mill (Eberl, 2003). Samples were dried overnight and shaken for 10 min with Vertrel solution, then passed again through a 150-μm sieve and mounted onto a side loading metal sample holder to maximize random mineral orientation (Whittig and Allardice, 1986). Samples were analyzed using a Scintag PAD-V powder X-ray diffractometer (Scintag, Inc. [currently Thermo Scientific], Cupertino, CA) with a Ge solid state detector and Cu-Ka radiation (Ka = 1.54178 Å). Voltage was set at 35 kV and current at 30 mA. Diffraction patterns were collected from 2 to 70° 2θ using a step size of 0.020° 2θ at 1° 2θ per minute. JADE software was employed to identify XRD peaks. Quantitative mineral abundance estimates were obtained from the resulting diffraction patterns using the USGS RockJock program (Eberl, 2003).

Clay Mineral Composition

For select soil samples, the clay fraction was separated by transferring the silt and clay suspension (<53-μm fraction) to 250-mL centrifuge bottles and centrifuged using a Sorvall Legend X1R Centrifuge (Thermo Fisher Scientific, Inc., Waltman, MA) at 750 rpm (11 ×g) for 7 min to settle the silt fraction (Jackson, 1974). The clay suspension was transferred to a clean 250-mL centrifuge bottle and centrifuged at 3000 rpm (171 × g) for 45 min. The clear supernatant was decanted and the remaining clays resuspended in approximately 40 mL of distilled water.

Clay mineral composition was obtained by treating the clay fraction with (i) ethylene glycol atmosphere at 60°C; (ii) K saturation with a 1 M KCl solution followed by heat treatments at 200, 350, and 530°C in a muffle furnace; (iii) Mg saturation with a 1 M $MgCl_2$ solution followed by treatment with glycerol; and (iv) acid (HCl) treatment (Jackson 1974; Poppe et al., 2002; Deng et al., 2009). Descriptions of the clay treatment methods are provided

in the Supplementary Material. Slides were prepared by pipetting roughly 2 mL of the treated clay and water suspension onto glass slides and air drying overnight. Diffraction patterns were obtained at the MCL using a PANalytical Empyrean X-ray diffractometer (Almelo, The Netherlands) with Cu-Ka radiation at 45 kV and 40 mA. Samples treated with ethylene glycol, K, Mg and HCl were scanned from 4 to 32° 2θ (scan time 7:48 min); heat-treated K saturated samples and glycerol treated Mg samples were scanned from 4 to 15° 2θ (scan time 3:09 min). A PIXcel detector was used in scanning mode with a position sensitive detector (PSD) length of 3.35° 2θ and 255 active channels. A 10-mm beam mask, a 1/4° divergence, and a 1/8° anti-scatter slit were used on the incident side of the diffractometer and a 1/16° anti-scatter slit and a 0.02-mm nickel filter were used on the diffracted side. A beam knife was used to minimize beam scatter at low angles.

RESULTS

Soil Morphology

Soils described across the climosequence are progressively more mature from north to south, as evidenced by increased development of subsurface diagnostic horizons, reddening, and increased clay accumulation (Fig. 1 and 2, Table S1). Soils in Wales

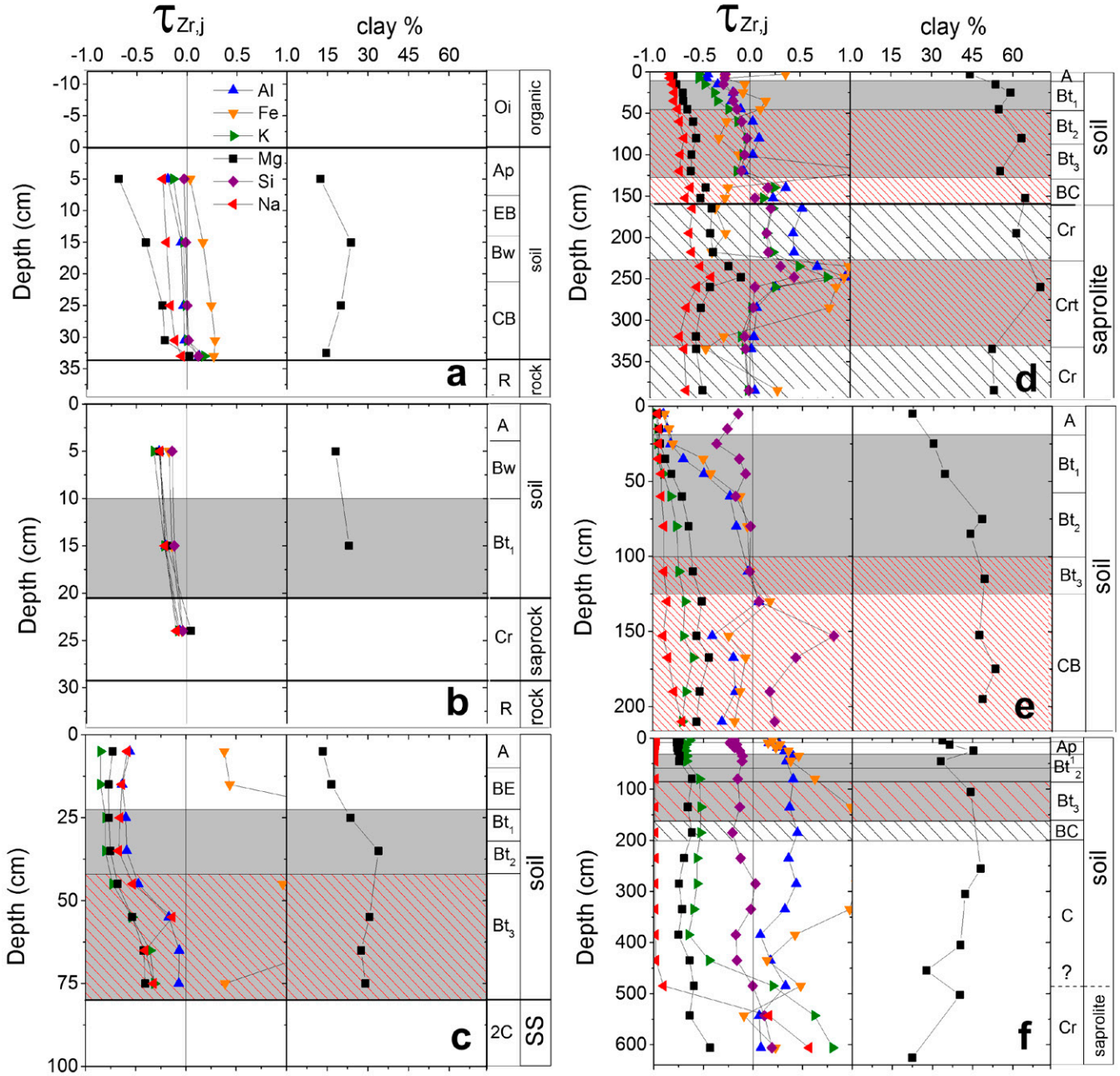

Fig. 2. Soil elemental τ profiles, clay content, and soil horizons as a function of depth at sites across the climosequence including (a) Wales, (b) Pennsylvania, (c) Virginia, (d) Tennessee, (e) Alabama, and (f) Puerto Rico. Gray shaded areas indicate the presence of clay films; no clay films were observed in unshaded areas. Sparsely hachured areas have a gleyed matrix with few to no concentrations while densely hachured areas have prominent redoximorphic features including both concentrations and depletions. Parent material is residual shale at all locations; weathered sandstone (SS) was observed below the weathered shale in the Virginia profile.

and PA are underlain by fractured shale bedrock (saprock; Fig. 2) which was not observed at the bottom of pits or soil cores at any other site (Fig. 2). The soil-saprolite boundary was difficult to identify in AL and PR; therefore the loss of pedogenic structure was used to define this boundary (Fig. 2). In TN, the saprolite boundary is more clearly defined at 160 cm where inherited shale structure was observed (Fig. 2). In VA, the soil profile (80 cm) developed from Rose Hill Formation shale that was intercalated with sandstone, resulting in more resistant sandstone clasts that are readily observed at the land surface (Fig. 2). In addition, it appears that weathering at this site has proceeded into the underlying sandstone unit and is visible at the base of the weathered shale profile, as observed at the base of the soil pit.

Minimal horizon development was observed in Wales and PA (Fig. 2). In PA, Bt horizons are weakly developed while soil profiles in VA, TN, AL, and PR exhibited well-developed Bt horizons (Fig. 2). Redoximorphic features, including both concentrations and depletions, were present in VA, TN, AL, and PR. The depth to redoximorphic features generally increases from 40 cm in VA to 45 cm in TN and 100 cm in AL, then decreases slightly to more weakly expressed redoximorphic features at 60 cm in PR. Redoximorphic features were most strongly expressed in the TN and AL soils. Total clay content generally increases from north to south across the climosequence, from approximately 20% in Wales to 50% at southern sites (Table 2, Fig. 2).

Soil Chemistry

Soil chemistry is reported in Table 3 for major elements Al, Ca, Fe, K, Mg, Mn, Na, P, Si, and the trace element Zr. Parent material elemental rock chemistry was previously reported in Dere et al. (2013). Concentrations of Si, Al, and Fe were greatest throughout all soil profiles while elements such as Ca and P were extremely low at all sites (Table 3).

The majority of elements exhibit depletion profiles whereby the mass transfer coefficient decreases toward the land surface (Brantley and White, 2009; Fig. 2). However, concentrations only return to parent composition at depth at the northern sites (Wales and PA), and to some extent, VA (Fig. 2). The majority of elements in TN, AL, and PR do not return to parent at the bottom of the sampled profile (Fig. 2). Sodium τ profiles were previously presented in Dere et al. (2013) and show depletion profiles at all sites, with the extent of depletion at the soil surface increasing from the northern (20–30% depletion in Wales and PA) to the southern end (100% depletions in PR) of the climosequence. Magnesium also exhibits depletion profiles and the extent of surface Mg depletion increases from north to south, although no sites are 100% depleted in Mg at the soil surface. Potassium is depleted from all soils but shows enrichment at depth in TN (Fig. 2). Iron is highly variable with depth and enriched in profiles at the Wales, VA, TN, and PR sites. Silicon is most variable in AL, where chert fragments inherited from the parent shale at this site were abundant (Dere et al., 2013). In PR, Al was enriched throughout the entire profile with respect to initial parent concentrations (Fig. 2).

Rock and Soil Mineralogy

Parent shale mineralogy comprises mainly quartz, illite, and chlorite minerals with smaller quantities of plagioclase, potassium feldspar, and iron oxides (Table 4). Quantitative XRD showed that plagioclase generally constitutes < 12% of the parent mineralogy, which is consistent with plagioclase quantities calculated using parent Na concentrations (Dere et al., 2013; Table 4). Iron oxides and potassium feldspar also represent < 12% of the bulk parent mineralogy. A small amount of kaolinite (<5%) was measured in the VA, TN, and PR parent rocks but is not thought to be a primary mineral in the shale (Jin et al., 2010). The presence of small amounts of kaolinite may indicate some weathering of the parent rock in the sampled outcrops. Illite is the dominant mineral in the PA parent material, comprising 63% of the parent mineralogy whereas the chlorite fraction is considerably smaller (5%) compared with all other parent rock samples (15–37% of the parent mineralogy) from the climosequence. The mineralogy of the PA sample reported here is consistent with the previous quantification of Rose Hill Formation shale mineralogy at SSHCZO located within 3 km from our study site (Jin et al., 2010).

In contrast to the other soils which contained $\leq$2% calcite, the parent shale in PR contains up to 45% calcite. This large difference in composition is not unexpected given the different depositional history of the shale at this site (Tobish and Turner, 1971). Calculations of calcite content based on bulk Ca concentrations (i.e., assuming all Ca is present only as calcite) are similar to estimates from quantitative XRD analysis for PR (47%) and TN (1.5%). In VA and AL, calcite determined from XRD analysis is slightly higher than calcite determined from Ca concentration in the shale (Table 4). No calcite was reported for quantitative XRD analysis in Wales and PA although bulk Ca concentrations equate to 0.19% calcite in PA and 0.08% calcite in Wales, assuming all Ca is carbonate derived. The most likely interpretation is Ca in PA and Wales is also present as plagioclase feldspar, which is known to be present. Overall, quantitative XRD analyses of calcite are in good agreement with bulk Ca concentrations, assuming any Ca in the bedrock is present largely as calcite.

Throughout the climosequence, the mineralogy of the bulk soils largely reflects the parent mineralogy with the addition of secondary minerals such as kaolinite, iron oxides, and vermiculite and loss of some weathered phases including calcite (PR), plagioclase, and illite (Fig. 3; Table 2). Total vermiculite/HIV content at the surface of the soil profiles increases from north to south, from ~8% in PA to 37% in PR. Similarly, all soils show kaolinite addition in the uppermost soil samples, with surface kaolinite content increasing toward the south (~6% in Wales to 30% in PR; Table 2). The disappearance of plagioclase from the surface soil is most evident in the PR profile, where plagioclase content decreases from 19% at the base of the profile and in the shale, to <1% plagioclase toward the soil surface. Potassium feldspar shows little change throughout the soil profiles in Wales, PA, and VA; in contrast, soil K feldspar decreases to-

Table 2. Soil depth, particle-size and mineralogy for select samples at each site.

Site	Sample	IGSN†	Depth	Sand	Silt	Clay	Quartz	K feldspar	Plagioclase	Illite	Vermiculite/HIV	Kaolinite	Iron oxides	Calcite
			cm	%										
Wales	PlynQ0–10	SSH000SSM	0–10	73	15	12	31	5.8	3.4	36	15.6	6.1	3.0	0.0
	PlynQ20–30	SSH0000HF	20–30	49	31	20	32	3.1	3.3	33	26.6	1.0	1.7	0.0
	PlynQ31–35	SSH0000HH	31– 35	60	25	15	31	1.2	4.4	38	25.0	–	0.8	0.0
PA	ALD-10–163	SSH0000NL	0–10	64	18	18	30	2.6	0.7	49	8.3	1.5	3.8	0.0
	ALD-10–164	SSH0000NM	10–20	63	14	23	27	2.1	0.5	59	10	0.6	1.9	0.0
	ALD-10–165	SSH0000NN	20–28	–	–	–	26	0.8	0.1	59	4.5	1.8	2.3	0.0
VA	MT-09–032	SSH0000PH	0–10	53	33	14	69	4.5	0.8	7.3	7.5	3.6	5.9	0.0
	MT-09–034	SSH0000PJ	20–30	51	25	24	–	–	–	–	–	–	–	–
	MT-09–036	SSH0000PL	40–50	44	22	34	73	3.2	0.8	16	0.9	0.5	5.8	0.0
	MT-09–038	SSH0000PN	60– 70	49	20	31	53	3.0	0.7	28	5.0	2.3	7.5	0.0
	MT-09–039	SSH0000PO	70– 80	53	20	27	55	1.4	1.6	37	0.0	1.8	2.7	0.0
TN	ALD-09–17	SSH0000QC	0–5	20	36	44	40	1.6	0.9	35	12	4.1	6.6	0.0
	ALD-09–03	SSH0000QH	20–30	14	32	54	33	1.3	0.0	47	6.3	7.2	5.6	0.0
	ALD-09–05	SSH0000QJ	40–50	14	31	55	33	1.2	0.7	46	6.8	6.9	5.8	0.0
	ALD-09–09	SSH0000QN	80–90	2.0	35	63	25	3.0	0.0	49	15	7.7	0.8	0.0
	ALD-09–13	SSH0000QR	120–130	14	31	55	25	1.4	0.9	45	11	7.2	10	0.0
	ALD-09–16	SSH0000QU	150–155	4.0	32	64	26	1.1	0.0	55	9.1	8.6	0.6	0.0
	ALD-10–67	SSH0000R1	190–200	1	38	61	24	3.5	0.0	53	9.8	10	0.0	0.0
	ALD-11–401	SSH0000RP	260–270	11	19	70	20	3.6	0.4	54	10	8.0	4.2	0.0
	ALD-11–426	SSH0000RW	330–340	6.0	42	52	25	4.5	0.3	47	12	9.9	1.5	0.0
	ALD-11–432	SSH0000S2	390–398	13	34	53	27	3.4	0.6	50	9.8	6.2	2.9	0.0
AL	ALD-10–114	SSH0000T3	0–10	37	41	22	83	4.4	1.0	7.4	1.6	1.6	1.2	0.0
	ALD-10–116	SSH0000T5	20–30	29	41	30	70	2.5	0.1	7.2	7	9.9	2.8	0.0
	ALD-10–121	SSH0000TA	60–70	17	35	48	39	2.6	0.9	5.4	24	22	5.8	0.0
	ALD-10–125	SSH0000TE	110–120	16	35	49	32	3.3	0.6	15	14	27	7.1	0.0
	ALD-10–129	SSH0000TI	150–155	19	34	47	65	2.4	0.7	18	4	7.4	3.0	0.0
	ALD-11–506	SSH0000TP	170–180	16	31	53	55	2.0	0.5	25	7.3	6.0	4.7	0.0
	ALD-11–508	SSH0000TR	190–200	15	37	48	50	2.8	0.7	15	16	13	2.7	0.0
PR	ALD-11–13	SSH0000VO	0–8	30	36	34	25	5.7	0.0	0.0	37	30	3.6	0.0
	ALD-11–19	SSH0000VU	40–50	25	42	33	27	2.5	0.0	0.0	31	33	7.1	0.0
	ALD-11–25	SSH0000W0	100–111	6.0	50	44	17	1.4	0.6	2.2	38	33	8.2	0.0
	ALD-11–43	SSH0000WF	250–260	15	37	48	21	3.3	0.0	0.0	38	27	10	0.0
	ALD-11–48	SSH0000WK	300–310	24	34	42	27	3.4	0.0	0.0	30	30	9.0	0.0
	ALD-11–58	SSH0000WU	400–410	30	29	41	30	2.9	0.0	2.3	29	28	7.9	0.0
	ALD-11–76	SSH0000X5	500–505	21	39	40	24	8.8	0.0	3.5	33	26	4.3	0.0
	ALD-11–92	SSH0000XL	625–632	52	25	23	25	20	19	3.0	26	5.3	1.2	0.0

† International Geo Sample Number, www.geosamples.org

Table 3. Major elemental soil chemistry and Zr concentrations across the climosequence. Some elements were below detection limit (BDL).

Site	IGSN†	Sample	d	Al	Ca	Fe	K	Mg	Mn	Na	P	Si	Ti	Zr
			cm	%										ppm
Wales	SSH000SSM	plnq0–10	0–10	8.89	0.02	6.27	2.37	0.43	0.17	0.47	0.08	22.9	0.56	166
	SSH0000HE	plnq10–20	10–20	10.5	0.02	7.13	2.67	0.80	0.46	0.50	0.05	23.6	0.56	168
	SSH0000HF	plnq20–30	20–30	11.0	0.02	7.83	2.81	1.06	0.40	0.53	0.05	24.5	0.55	172
	SSH0000HG	plnq30–31	30–31	11.0	0.03	7.97	2.82	1.07	0.36	0.56	0.07	24.6	0.53	170
	SSH0000HH	plnq31–35	31–35	11.7	0.03	7.34	3.06	1.31	0.44	0.56	0.04	25.0	0.55	158
PA	SSH00001Q	ALD–10–163	0–10	10.8	0.02	5.17	3.77	0.60	0.16	0.21	0.08	27.1	0.71	216
	SSH00001R	ALD–10–164	10–20	11.5	0.01	5.21	4.26	0.65	0.02	0.22	0.06	27.1	0.72	211
	SSH00001S	ALD–10–165	20–30	12.2	0.03	5.25	4.51	0.75	0.01	0.22	0.07	26.8	0.70	190
VA	SSH0000PH	MT–09–032	0–10	3.26	0.07	2.32	0.37	0.18	1.56	0.06	0.07	33.8	0.50‡	–
	SSH0000PI	MT–09–033	10–20	2.66	0.04	2.27	0.41	0.16	0.43	0.06	0.05	33.5	0.50	–
	SSH0000PJ	MT–09–034	20–30	3.03	0.04	2.69	0.56	0.17	0.36	0.07	0.05	38.6	0.39	–
	SSH0000PK	MT–09–035	30–40	2.94	0.05	2.48	0.46	0.17	0.58	0.06	0.07	37.6	0.38	–
	SSH0000PL	MT–09–036	40–50	3.98	0.03	3.28	0.86	0.21	0.25	0.07	0.06	36.6	0.47	–
	SSH0000PM	MT–09–037	50–60	6.14	0.04	4.70	1.41	0.30	0.15	0.08	0.06	32.9	0.43	–
	SSH0000PN	MT–09–038	60–70	6.30	0.04	5.39	1.93	0.33	0.04	0.07	0.11	32.7	0.47	–
	SSH0000PO	MT–09–039	70–80	6.14	BDL	3.43	1.99	0.35	0.03	0.08	0.05	34.6	0.52	–
TN	SSH0000QC	ald–09–17	0–5	7.25	0.02	7.48	2.38	0.40	0.03	0.13	0.09	25.4	0.62	315
	SSH0000QD	ald–09–18	5–10	8.46	0.01	4.94	2.82	0.48	0.03	0.15	0.05	30.1	0.74	375
	SSH0000QG	ald–09–02	10–20	9.42	0.03	5.82	2.96	0.50	0.06	0.16	0.07	27.6	0.70	350
	SSH0000QH	ald–09–03	20–30	10.2	0.01	5.06	3.07	0.55	0.15	0.15	0.05	27.8	0.67	310
	SSH0000QI	ald–09–04	30–40	9.73	0.01	6.09	3.10	0.54	0.07	0.14	0.06	26.8	0.65	300
	SSH0000QJ	ald–09–05	40–50	10.3	0.01	5.51	3.45	0.58	0.01	0.16	0.05	26.6	0.64	285
	SSH0000QL	ald–09–07	60–70	11.4	0.01	3.76	3.79	0.66	BDL	0.16	0.04	27.6	0.64	280
	SSH0000QN	ald–09–09	80–90	1.5	BDL	3.21	3.94	0.66	BDL	0.18	0.03	27.6	0.64	265
	SSH0000QP	ald–09–11	100–110	11.0	BDL	4.21	3.85	0.61	BDL	0.16	0.04	27.4	0.64	270
	SSH0000QR	ald–09–13	120–130	9.47	BDL	10.1	3.40	0.57	BDL	0.15	0.08	25.0	0.59	255
	SSH0000QT	ald–09–15	145–150	11.6	BDL	2.94	4.11	0.65	BDL	0.17	0.02	27.1	0.62	215
	SSH0000QU	ald–09–16	150–155	12.0	BDL	3.22	4.27	0.67	BDL	0.17	0.03	27.6	0.64	245
	SSH0000QY	ald–10–64	160–170	12.6	0.00	2.40	3.94	0.70	0.00	0.18	0.03	27.1	0.61	209
	SSH0000R1	ald–10–67	190–200	12.4	0.00	2.90	3.92	0.71	0.00	0.17	0.03	27.3	0.62	218
	SSH0000R4	ald–10–70	210–220	12.4	0.01	2.36	4.10	0.74	0.01	0.18	0.03	27.6	0.63	217
	SSH0000R8	ald–10–73	230–240	11.9	0.01	6.27	4.11	0.77	0.01	0.18	0.04	25.1	0.57	180
	SSH0000R9	ald–10–75	240–250	12.4	0.00	5.45	4.36	0.79	0.08	0.19	0.04	24.7	0.56	160
	SSH0000RP	ald–11–401	260–270	12.4	0.02	7.82	4.39	0.79	0.01	0.19	0.06	26.9	0.56	230
	SSH0000RS	ald–11–404	290–300	10.1	0.01	7.48	3.72	0.66	0.01	0.17	0.05	26.3	0.60	238
	SSH0000RW	ald–11–426	330–340	11.1	0.02	3.50	3.79	0.67	0.02	0.16	0.04	27.5	0.63	270
	SSH0000RZ	ald–11–429	360–370	11.1	0.01	2.71	4.03	0.69	0.03	0.19	0.04	28.3	0.63	277
	SSH0000S2	ald–11–432	390–398	10.6	0.01	5.68	3.83	0.73	0.05	0.18	0.05	27.0	0.61	254
AL	SSH0000T3	ald–10–114	0–10	1.93	0.09	1.22	0.28	0.10	0.09	0.02	0.04	41.6	0.25	314
	SSH0000T4	ald–10–115	10–20	2.71	0.04	1.74	0.38	0.13	0.21	0.02	0.04	38.3	0.39	331
	SSH0000T5	ald–10–116	20–30	3.83	0.04	2.45	0.44	0.18	0.07	0.03	0.04	37.7	0.43	380
	SSH0000T6	ald–10–117	30–40	4.59	0.05	4.31	0.48	0.21	0.05	0.02	0.06	35.6	0.38	265
	SSH0000T7	ald–10–118	40–50	6.82	0.04	4.39	0.61	0.28	0.09	0.02	0.05	33.9	0.42	236
	SSH0000TA	ald–10–121	60–70	9.76	0.03	6.29	0.98	0.41	0.02	0.02	0.08	28.7	0.44	224
	SSH0000TC	ald–10–123	90–100	9.31	0.05	6.00	1.15	0.45	0.02	0.02	0.07	29.9	0.40	197
	SSH0000TE	ald–10–125	110–120	10.1	0.04	5.85	1.20	0.47	0.01	0.02	0.08	28.1	0.41	187
	SSH0000TG	ald–10–127	130–140	10.1	0.04	6.34	1.33	0.52	0.02	0.03	0.08	27.6	0.43	168
	SSH0000TI	ald–10–129	150–155	4.33	0.02	3.14	0.96	0.35	0.01	0.01	0.04	36.2	0.24	129
	SSH0000TP	ald–10–506	170–180	6.97	0.03	4.57	1.51	0.54	0.01	0.03	0.06	33.9	0.38	153
	SSH0000TR	ald–10–508	190–200	8.03	0.04	4.82	1.39	0.51	0.10	0.04	0.07	31.2	0.39	172
	SSH0000TT	ald–11–510	200– 210	6.72	0.02	4.51	1.24	0.47	0.02	0.06	0.05	32.5	0.37	172

Table 3. Continued.

Site	IGSN†	Sample	d	Al	Ca	Fe	K	Mg	Mn	Na	P	Si	Ti	Zr
			cm	%										ppm
PR	SSH0000VO	ald–11–13	0–8	9.58	0.78	5.85	0.51	0.58	0.02	0.05	0.10	22.5	0.48	139
	SSH0000VP	ald–11–14	8–10	10.4	0.59	6.18	0.47	0.56	0.02	0.04	0.08	23.2	0.50	153
	SSH0000VQ	ald–11–15	10–15	10.6	0.56	6.34	0.46	0.56	0.02	0.04	0.08	23.4	0.50	142
	SSH0000VR	ald–11–16	15–20	10.9	0.49	6.47	0.45	0.55	0.02	0.03	0.08	24.2	0.51	150
	SSH0000VS	ald–11–17	20–30	11.0	0.44	6.79	0.45	0.54	0.01	0.03	0.07	24.4	0.51	142
	SSH0000VT	ald–11–18	30–40	11.1	0.42	6.90	0.44	0.55	0.01	0.02	0.07	23.8	0.49	134
	SSH0000VU	ald–11–19	40–50	11.0	0.42	6.82	0.46	0.57	0.01	0.02	0.08	24.8	0.50	141
	SSH0000W0	ald–11–25	100–111	10.7	0.45	7.43	0.60	0.79	0.01	0.03	0.07	21.8	0.54	130
	SSH0000W5	ald–11–30	150–160	10.7	0.23	9.32	0.63	0.72	0.02	0.02	0.07	22.9	0.53	133
	SSH0000WA	ald–11–38	200–210	11.2	0.13	11.51	0.62	0.80	0.02	0.02	0.06	20.7	0.51	132
	SSH0000WF	ald–11–43	250–260	10.1	0.09	12.78	0.55	0.60	0.02	0.02	0.08	22.0	0.49	127
	SSH0000WK	ald–11–48	300–310	10.3	0.06	8.72	0.53	0.48	0.02	0.02	0.09	24.7	0.46	122
	SSH0000WP	ald–11–53	350–360	9.86	0.06	8.82	0.51	0.57	0.04	0.02	0.11	24.7	0.45	127
	SSH0000WU	ald–11–58	400–410	9.76	0.10	7.74	0.54	0.60	0.03	0.03	0.09	25.4	0.51	155
	SSH0000WZ	ald–11–63	450–460	10.5	0.11	6.11	0.85	0.86	0.02	0.04	0.08	25.3	0.60	152
	SSH0000X5	ald–11–76	500–505	9.91	0.26	6.62	1.53	0.81	0.02	0.15	0.09	25.1	0.56	127
	SSH0000XF	ald–11–86	570–580	8.12	0.43	4.16	2.11	0.74	0.02	1.78	0.09	28.8	0.53	130
	SSH0000XL	ald–11–92	625–632	7.58	0.64	5.16	2.16	1.07	0.03	2.20	0.09	28.2	0.53	120

† International Geo Sample Number, www.geosamples.org.

‡ VA corrected Ti values as reported in Dere et al. (2013).

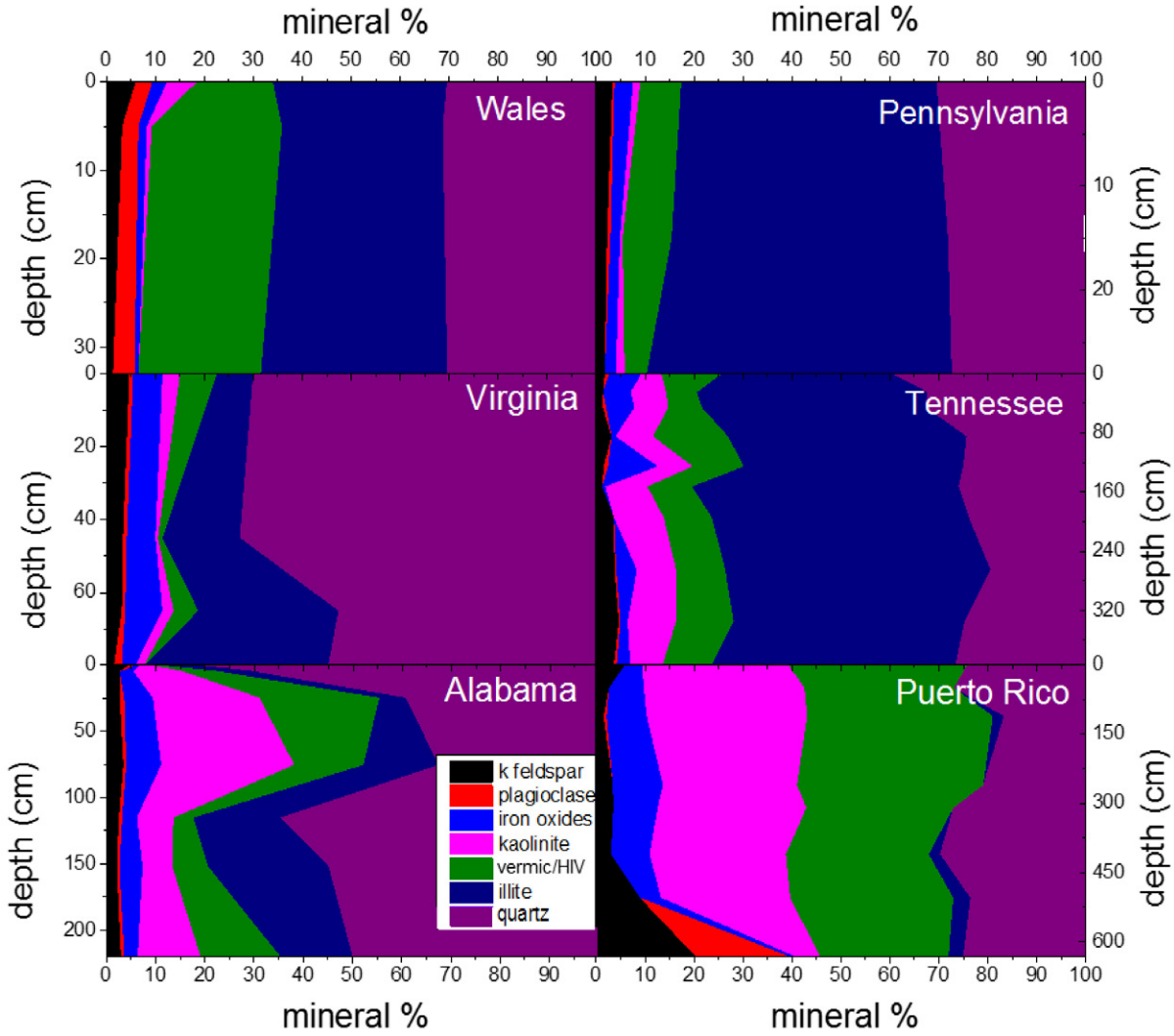

Fig. 3. Bulk soil mineralogy as a function of depth across the climosequence. Vermic/HIV includes vermiculite and hydroxy-interlayered vermiculite minerals.

Table 4. Shale bedrock mineralogy for select samples at each site.

Site	Sample	IGSN†	Quartz	K feldspar	Plagioclase	Illite	Chlorite	Kaolinite	Iron oxides	Calcite
						%				
Wales	PlynQ-RF	SSH000GG	30	1.1	4.0	39	25	–	0.70	–
PA	ALD-10–58	SSH000SUA	26	2.4	0.5	63	4.6	–	3.8	–
VA	TSW1164	SSH00005D	19	2.7	3.1	40	26	4.6	4.0	0.60
TN	TSW1208	SSH00006M	28	4.1	5.5	29	22	4.2	5.6	1.1
AL	ALD-10–2026	SSH00008K	16	6.2	1.3	30	37	–	7.4	2.2
PR	ALD-11–03	SSH000SUW	14	9.0	12	2.6	15	1.6	0.40	45

† International Geo Sample Number, www.geosamples.org.

ward the soil surface in TN, AL, and PR. Iron oxide content generally increases toward the soil surface, consistent with previous observations of iron oxide minerals in SSHCZO (Yesavage et al., 2012). However, Fe shows high variability with depth, especially in the southern profiles (TN, AL, and PR).

Soil Clay Mineral Composition

In addition to quantitative XRD, we completed a more detailed analysis of mineralogy in the clay (<2 μm) fraction for selected soils across the climosequence. At all sites, minerals present in the clay fraction include illite, vermiculite, quartz, and kaolinite (Fig. S2–S6). None of the studied soil samples contain smectite as evidenced by the fact that no changes were observed in the apparent d-spacing of the 14-Å peak following solvation of a Mg-saturated sample with glycerol (Moore and Reynolds, 1997). Soil samples treated with 1 M HCl confirmed the presence of kaolinite at all sites. Vermiculite in the clay fraction of samples from VA (Fig. S3), TN (Fig. S4), and AL (Fig. S6) contains hydroxy-interlayers, as indicated by the incomplete collapse of the 14-Å peak with K-saturation. Successive heat treatments of these samples, up to 530°C, result in progressive collapse of the clay toward a 10-Å d-spacing.

The clay diffraction patterns highlight the weathered nature of the 14-Å minerals. Wales is the only site where discrete chlorite is positively identified in the soil clay fraction by the persistence of the 14-Å peak even after K saturation and heating to 530°C (Fig. S2). At all other sites, the 14-Å peak shifts toward 10-Å with K-saturation and heat treatments, indicating the presence of vermiculite or HIV, or both. Both vermiculite and hydroxy-interlayerd vermiculite are common weathering products of chlorite in soil environments (Dixon and Weed, 1977). A small peak at 3.2 Å in the sample from Wales could indicate the presence of albite in the clay fraction, whereas the 4.7-Å and 4.5-Å peaks observed only at this site could be secondary reflections of chlorite and vermiculite, respectively (Harris and White, 2008).

DISCUSSION

Throughout the climosequence Na is largely present in plagioclase feldspar that weathers to kaolinite. Given that no other Na-bearing minerals were identified through XRD and the fact that Na is not taken up appreciably by vegetation (Herndon et al., 2015), we conclude that the dissolution of plagioclase results in the loss of Na as solute from the weathered profile. Indeed, the extent of observed Na loss is consistent with enhanced plagioclase weathering as temperatures increase across the climosequence (Dere et al., 2013). Although plagioclase constitutes <12% of the initial shale and we cannot conclusively identify the true depth to which Na is depleted in each profile, this weathering reaction is the first and deepest reaction we identify (without drilled samples) in the weathering profile. Such an interpretation is consistent with work by Jin et al. (2010) at the PA SSHCZO, which lies within 3 km of our sampled site, where analysis of shale chips in the soil revealed depletion of Na, but not of other elements present in clay minerals (K, Mg, Al, Fe). Thus plagioclase dissolution occurred deeper than measurable clay mineral dissolution. In this respect, plagioclase dissolution can be considered the so-called "regolith-initiating reaction", that is, the deepest reaction that occurs close to the point where bedrock disaggregates to grains <2 mm, roughly equivalent to the augerable soil depth at these sites (Brantley et al., 2013).

Previous work at the SSHCZO also identified several weathering reaction fronts in 20-m boreholes drilled into bedrock (Brantley et al., 2013). For example, under the northern ridge of SSHCZO, the deepest reaction is oxidative dissolution of pyrite, followed closely by dissolution of the carbonate mineral ankerite. All pyrite and ankerite are completely depleted by 23-m depth under the ridge. Weathering of plagioclase and illite commences at 6 and 0.5 m, respectively (Jin et al., 2010). Although we did not drill boreholes at our sites, it is possible that deep weathering reactions that remove pyrite and carbonate minerals also occur at depths > 20 m along the climosequence studied here. Given the lack of drilled samples along the climosequence, it is impossible to delineate pyrite and carbonate reaction fronts south of PA or conclude which reaction is profile-initiating. However, consistent with the carbonate depletion model, PR is 100% depleted of carbonate despite calcite constituting almost half of the parent shale (Table 4). Thus, the loss of Ca to 632 cm is inferred to represent the minimum depth of calcite dissolution at this site. Calcite is an extremely small proportion of shale at all other sites (0–2%) and is often absent (below detection) in soils, indicat-

ing that the small fraction of calcite present in parent material at these sites may also have dissolved.

In the shale bedrock, Mg is largely found in chlorite minerals, and to a lesser extent illite (<5%; Jin et al., 2010). Smectite minerals, which can also contain Mg, were not observed in any soils across the climosequence, as expected for the humid climate regimes included in this study (Barshad, 1966; Barshad and Kishk, 1969; Helgeson et al., 1969). The proportion of vermiculite/HIV in the soils increases from north to south, indicating a greater transformation of clay minerals in the bedrock to secondary clay minerals in the soil (Fig. 3). Wales is the only site with chlorite identified in the soils. Based on the lack of chlorite observed in soils at SSHCZO and all other sites along the climosequence, we assume vermiculite/HIV is the dominant secondary mineral resulting from weathering reactions at these sites.

The transformation of chlorite minerals, and to a lesser extent illite, to vermiculite or HIV complicates the interpretation of the Mg τ profiles because unlike Na, Mg can be retained in vermiculite and HIV secondary minerals rather than leaving the profile (Dixon and Weed, 1977; Chapman, 1986; Bain et al., 1993). In other words, it is difficult to interpret the proportion of Mg lost from the weathering of primary chlorite minerals because the weathering-derived Mg is not necessarily removed from the soil profile, but may be retained in vermiculite and HIV, maintaining $-1 < \tau$ surface < 0. Nonetheless, soils are increasingly Mg-depleted at the soil surface from north to south while the proportion of vermiculite/HIV at the land surface increases toward the south, consistent with the interpretation that Mg lost from chlorite minerals is retained in vermiculite and HIV (Fig. 2 and 3). The dissolution of chlorite, comprising roughly one third of the parent mineralogy, represents the dominant weathering reaction contributing to Mg loss and the transformation of chlorite to vermiculite and HIV in these profiles.

Typically, K is almost entirely present within illite minerals in shale-derived soils, transforming to vermiculite on weathering (Bain et al., 1993). Previous research characterizing the mineralogy of the Rose Hill Formation shale at the SSHCZO reported that illite loses more Fe than chlorite during ridgetop weathering (Yesavage et al., 2012) and is thought to weather before chlorite at this site (Jin et al., 2010). In addition, similar K and Mg depletion profiles at SSHCZO were attributed to the congruent dissolution of illite and chlorite (Jin et al., 2010). A similar observation describes K and Mg depletion profiles at most of our study sites, which we likewise attribute to simultaneous dissolution of chlorite and illite minerals. In Wales, however, Mg is more depleted than K throughout the soil profile, consistent with previous interpretations that chlorite weathers more rapidly than illite at this site (Chapman, 1986). Tennessee is anomalous in that K is half as depleted as Mg in the upper part of the profile and greatly enriched at depth (160–380 cm) before returning to parent composition at the bottom of the profile (Fig. 2). This may be the result of uneven clay mineral translocation into the saprolite fabric, as evidenced by an absence of clay films in the center of the profile (160–220 cm) and then recurrence of the clay films at the 220-cm depth (Fig. 2). Previous work in the area reported similar observations in saprolite and attributed the patterns to laterally transported clay material having moved along saprolite fractures at depth (Driese et al., 2001; McKay et al., 2005).

Kaolinite is a stable secondary mineral phase resulting from the destruction of minerals in the 2:1 clay family or the dissolution of plagioclase minerals (Berner and Berner, 1996) and is increasingly abundant at the soil surface toward the southern end of the climosequence (>30%), consistent with enhanced weathering at the southern sites (Fig. 3). The initial plagioclase content of PR bedrock is 12% but kaolinite constitutes up to 30% of the bulk mineralogy in the soils. Therefore kaolinite present in this soil must not only result from plagioclase dissolution but also clay mineral weathering.

Iron oxides are present in the unweathered shale at all sites but are also precipitated through the weathering of chlorite minerals. The contributions of iron oxides to the soil mineralogy do not show a clear trend with depth and is highly variable within each profile. However, iron oxides can be difficult to identify with XRD if crystallinity is poor (Kunze and Dixon, 1986). Furthermore, iron oxides appear to be mobilized as particulates rather than dissolved as solutes from shale weathering at the SSHCZO (Jin et al., 2010; Yesavage et al., 2012). Nonetheless, even with the observed variability, a greater percentage of iron oxides is present in the southern soils (up to 10% compared with <3% at northern sites), again consistent with more advanced weathering at these sites compared with the northern sites (Buol et al., 2003).

Quartz is not expected to be a very reactive mineral in these weathering systems and for some sites, including Wales, PA, and PR, the abundance of quartz does not vary much with depth (Table 2). In VA, TN, and AL, quartz abundance is greatest near the soil surface, possibly a result of relative quartz enrichment as other minerals are weathered. Alternatively, some quartz may result from the inclusion of sandstone material from the previously overlying sandstone units or the inclusion of chert in the shale at the AL site (Dere et al., 2013). In fact, Si is heavily enriched at the VA site where blocks of sandstone are present on the soil surface (Fig. 2).

In summary, the dominant weathering reactions in the sampled regolith profiles along the climosequence include: (i) plagioclase dissolution that produces kaolinite and releases Na ions that are lost in solution from the soil; and (ii) chlorite and illite transformations that produce vermiculite and HIV, which in turn weather to form kaolinite and iron oxides (Fig. 4). In PR, however, the dissolution of calcite is assumed to have occurred at depth beneath the soil; this reaction may also have occurred at depth at other sites. The deepest weathering reaction observed in the regolith at these shale sites was dissolution of plagioclase feldspar, which may be the profile initiating reaction that begins the transformation of shale bedrock to weathered regolith (Brantley et al., 2013). Although plagioclase dissolution may initiate weathering, this mineral constitutes a small fraction (<12%) of parent rock across the climosequence and therefore is unlikely

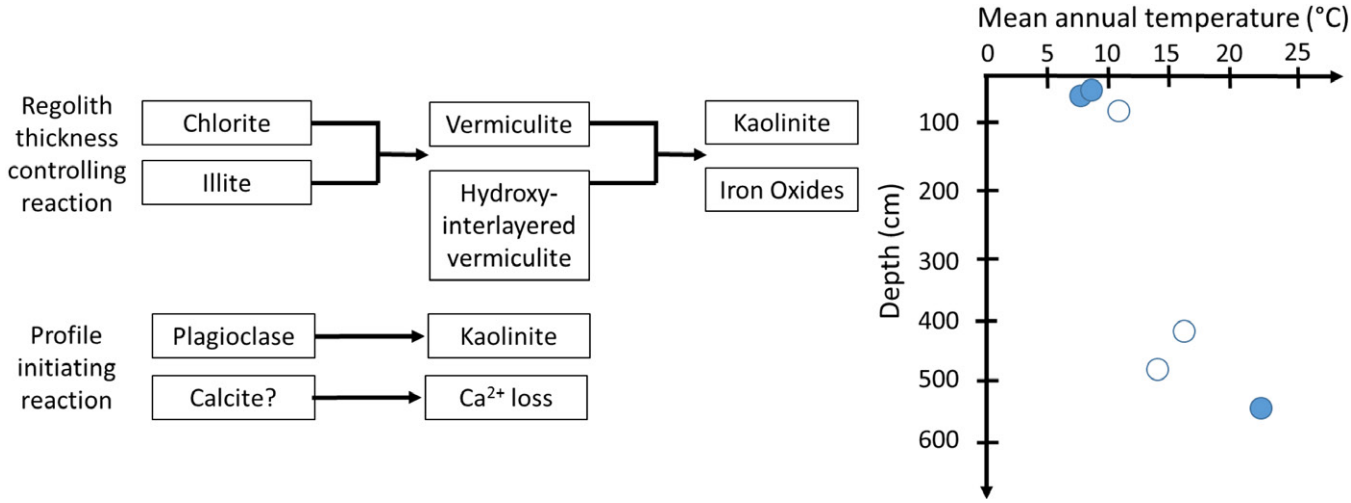

Fig. 4. Conceptual model of the main weathering reactions initiating soil profile development and controlling regolith thickness across the shale climosequence. Circles indicate estimated depth where plagioclase dissolution begins in each profile. Open circles represent reaction front depths estimated by fitting Na depletion curves (see Dere et al., 2013). Calcite is present in the Puerto Rico shale but is completely weathered from the soil profile, thus calcite dissolution may be the deepest weathering reaction at this site. Calcite dissolution may be occurring at depth at other sites in the climosequence, but calcite represents <2% of the initial mineral composition of the shale at these sites and we lack deep cores to confirm the maximum depth of this reaction front.

to control regolith thickness. The abundance of chlorite and its transformation to vermiculite and HIV are more likely controlling regolith thickness in these soils. Detailed characterization of the morphology, geochemistry, and mineralogy of shale-derived soils across a climosequence documents enhanced weathering and soil development with increasingly warm and wet climates; such characterization across a range of climate regimes will help us move toward a more quantitative understanding of the CZ.

ACKNOWLEDGMENTS

This work was funded by NSF Critical Zone Observatory grant EAR 07-25019 to C. Duffy, NSF GK-12 CarbonEARTH grant (EHR 094-47962) to R. Diehl, and a GSA Student Research Grant to A. Dere. We also thank the Centre for Ecology and Hydrology, especially B. Reynolds, S. Grant, D. Robinson, I. Robinson, D. Norris, and B. Emmett, for assistance with Plynlimon samples. We thank H. Gong, M. Safer, and L. Liermann for analytical assistance at Penn State. The authors are grateful for field assistance from: A. Adames-Corraliza, N. Bingham, G. Carlson, D. Dere, K. Downey, T. Frederick, M. Friday, L. Jin, D. Harbor, E. Heider, D. Keller, E. Knapp, K. Lease, L. Leidel, S. Lemon, L. Mann, G. Marshall, L. McKay, T. Miller, J. Moskal, J. Morales, R. Ruiz-Velez, M. Townsend, L. Vazguez-Albelo, D. Vazguez-Ortiz, M. Wagaw, F. Washington, N. West, D. Wilson, and J. Williams. This work also greatly benefitted from discussions with M. Carter, P. Grieve, X. Gu, E. Herndon, L. Jin, S. Hyneck, L. Ma, J. Orlando, G. Steinhoefl, P. Sullivan, N. West, and T. Yesavage.

SUPPLEMENTAL MATERIAL

Supplemental material includes detailed methodology for clay mineral X-ray diffraction. Supplemental figures include particle-size distribution with depth and clay mineralogy diffractograms. Supplemental tables include soil profile descriptions.

REFERENCES

April, R.H., M.M. Hluchy, and R.M. Newton. 1986. The nature of vermiculite in Adirondack soils and till. Clays Clay Miner. 34:549–556. doi:10.1346/CCMN.1986.0340508

Amundson, R. 2004. Soil formation. In: J.I. Drever et al., editors, Treatise in geochemistry. Elsevier, Amsterdam. p. 1–35.

Anderson, S.P., W.E. Dietrich, and G.H. Brimhall. 2002. Weathering profiles, mass-balance analysis, and rates of solute loss: Linkages between weathering and erosion in a small, steep catchment. Geol. Soc. Am. Bull. 114:1143–1158.

Bain, D.C., A. Mellor, M.S.E. Robertson-Rintoul, and S.T. Buckland. 1993. Variations in weathering processes and rates with time in a chronosequence of soils from Glen Feshie, Scotland. Geoderma 57:275–293. doi:10.1016/0016-7061(93)90010-I

Banwart, S., S.M. Bernasconi, J. Bloem, W. Blum, M. Brandao, S. Brantley, et al. 2011. Soil processes and functions in Critical Zone Observatories: Hypotheses and experimental design. Vadose Zone J. 10:974–987. doi:10.2136/vzj2010.0136

Barshad, I. 1966. The effect of variation in precipitation on the nature of clay minerals formation in soils from acid and basic igneous rocks. Proc. Int. Clay Congr. Jerusalem, Israel. 1:167-173.

Barshad, I., and F.M. Kishk. 1969. Chemical composition of soil vermiculite clays as related to their genesis. Contrib. Mineral. Petrol. 24:136–155. doi:10.1007/BF00376887

Bazilevskaya, E., M. Lebedeva, M. Pavich, G. Rother, D.Y. Parkinson, D. Cole, and S.L. Brantley. 2013. Where fast weathering creates thin regolith and slow weathering creates thick regolith. Earth Surf. Processes Landforms 38:847–858. doi:10.1002/esp.3369

Bazilevskaya, E., G. Rother, D.F.R. Mildner, M. Pavich, D. Cole, M.P. Bhatt, L. Jin, C.I. Steefel, and S.L. Brantley. 2015. How oxidation and dissolution in diabase and granite control porosity during weathering. Soil Sci. Soc. Am. J. 79:55–73. doi:10.2136/sssaj2014.04.0135

Behrens, R., J. Bouchez, J.A. Schuessler, S. Dultz, T. Hewawasam, and F. von Blanckenburg. 2015. Mineralogical transformations set slow weathering rates in low-porosity metamorphic bedrock on mountain slopes in a tropical climate. Chem. Geol. 411:283–298. doi:10.1016/j.chemgeo.2015.07.008

Berner, E.K., and R.A. Berner. 1996. Global environment: Water, air and geochemical cycles. Prentice Hall, Inc., New Jersey.

Birkeland, P.W. 1999. Soils and geomorphology. Oxford Univ. Press, New York.

Bockheim, J.G., J.S. Munroe, D. Douglass, and D. Koerner. 2000. Soil development along an elevational gradient in the southeastern Uinta Mountains, Utah, USA. Catena 39:169–185. doi:10.1016/S0341-8162(99)00091-0

Brantley, S.L., J. Bandstra, J. Moore, and A.F. White. 2008. Modelling chemical depletion profiles in regolith. Geoderma 145:494–504. doi:10.1016/j.geoderma.2008.02.010

Brantley, S.L., and M. Lebedeva. 2011. Learning to read the chemistry of the regolith to understand the critical zone. Annu. Rev. Earth Planet. Sci. 39:387–416. doi:10.1146/annurev-earth-040809-152321

Brantley, S.L., M.B. Goldhaber, and K.V. Ragnarsdottir. 2007. Crossing disciplines and scales to understand the Critical Zone. Elements 3:307–

314. doi:10.2113/gselements.3.5.307
Brantley, S.L., M.E. Holleran, L. Jin, and E. Bazilevskaya. 2013. Probing deep weathering in the Shale Hills Critical Zone Observatory, Pennsylvania (USA): The hypothesis of nested chemical reaction fronts in the subsurface. Earth Surf. Processes Landforms 38:1280–1298. doi:10.1002/esp.3415
Brantley, S.L., and A.F. White. 2009. Approaches to modeling weathered regolith. Rev. Mineral. Geochem. 70:435–484. doi:10.2138/rmg.2009.70.10
Brimhall, G.H., and W.E. Dietrich. 1987. Constitutive mass balance relations between chemical composition, volume, density, porosity, and strain in metasomatic hydrochemical systems: Results on weathering and pedogenesis. Geochim. Cosmochim. Acta 51:567–587. doi:10.1016/0016-7037(87)90070-6
British Geological Survey. 2005. Digital geological map of Great Britain. Version 1.11.British Geological Survey, Keyworth, Nottingham. Tile TQ69SW. Release date 20-04-2005. 1:10 000 scale (DiGMapGB-10) data [CD-Rom].
Buol, S.W., R.J. Southard, R.C. Graham, and P.A. McDaniel. 2003. Soil genesis and classification. 5th ed. Iowa State Press, Iowa.
Buss, H.L., P.B. Sak, S.M. Webb, and S.L. Brantley. 2008. Weathering of the Rio Blanco quartz diorite, Luquillo Mountains, Puerto Rico: Coupling oxidation, dissolution, and fracturing. Geochim. Cosmochim. Acta 72:4488–4507. doi:10.1016/j.gca.2008.06.020
Buurman, P., T. Pape, and C.C. Muggler. 1997. Laser grain-size determination in soil genetic studies 1. Practical problems. Soil Sci. 162:211–218. doi:10.1097/00010694-199703000-00007
Cadwell, D.H., and E.H. Muller. 2004. New York glacial geology, U.S.A. In: J. Ehlers and P.L. Gibbard, editors, Quaternary glaciations—Extent and chronology. Part II: North America. Elsevier, Netherlands. p. 201–205.
Catt, J.A., P.L. Gibbard, J.J. Lowe, D. McCarroll, J.D. Scourse, M.J.C. Walker, and J.J. Wymer. 2006. Quaternary: Ice sheets and their legacy. In: P.J. Brenchley and P.F. Rawson, editors, The geology of England and Wales. The Geological Society of London, London. p. 429–467.
Chadwick, O.A., R.T. Gavenda, E.F. Kelly, K. Ziegler, C.G. Olson, W.C. Elliott, and D.M. Hendricks. 2003. The impact of climate on the biogeochemical functioning of volcanic soils. Chem. Geol. 202:195–223. doi:10.1016/j.chemgeo.2002.09.001
Chapman, P. 1986. Geochemical and mineralogical studies of the weathering of Silurian argillaceous rocks. Ph.D. Diss. Univ. of North Wales, Bangor.
Clark, G.M., and E.J. Ciolkosz. 1988. Periglacial geomorphology of the Appalachian highlands and interior highlands south of the glacial border—A review. Geomorphology 1:191–220. doi:10.1016/0169-555X(88)90014-1
Ciolkosz, E.J., R.C. Cronce, and W.D. Sevon. 1986. Periglacial features in Pennsylvania. Agron. Ser. 92. Pennsylvania State Univ., University Park, PA.
Dahlgren, R.A., J.L. Boettinger, G.L. Huntington, and R.G. Amundson. 1997. Soil development along an elevational transect in the western Sierra Nevada, California. Geoderma 78:207–236. doi:10.1016/S0016-7061(97)00034-7
Deng, Y., G.N. White, and J.B. Dixon. 2009. Soil mineralogy laboratory manual. 11th ed. Dep. of Soil and Crop Sciences, Texas A&M Univ., College Station, TX.
Dere, A.L., T.S. White, R.H. April, B. Reynolds, T.E. Miller, E.P. Knapp, L.D. McKay, and S.L. Brantley. 2013. Climate dependence of feldspar weathering along a latitudinal gradient. Geochim. Cosmochim. Acta 122:101–126. doi:10.1016/j.gca.2013.08.001
Dixon, J.B., and S.B. Weed. 1977. Minerals in soil environments. Soil Sci. Soc. Amer. Madison, WI.
Dokuchaev, V.V. 1883. Russian chernozems (Russkii chernozem). Israel Prog. Sci. Trans., Jerusalem, 1967. Transl. from Russian by N. Kraner. Available from U.S. Dep. Of Commerce, Springfield, VA.
Driese, S.G., L.D. McKay, and C.P. Penfield. 2001. Lithologic and pedogenic influences on porosity distribution and groundwater flow in fractured sedimentary saprolite: A new application of environmental sedimentology. J. Sediment. Res. 71:843–857. doi:10.1306/2DC4096D-0E47-11D7-8643000102C1865D
Eberl, D.D. 2003. User's guide to RockJock– A program for determining quantitative mineralogy from powder x-ray diffraction data. U.S. Geological Survey, Open-file report 2003-78. U.S. Geological Survey, Boulder, CO.
Egli, M., A. Mirabella, G. Sartori, and P. Fitze. 2003. Weathering rates as a function of climate: Results from a climosequence of the Val Genova (Trentino, Italian Alps). Geoderma 111:99–121. doi:10.1016/S0016-7061(02)00256-2
Finlayson, C.P. 1964. Geology map and mineral resources summary of the White Hollow quadrangle. Geologic Map GM-145-SW. Tennessee. Tennessee Div. Geol., Nashville, TN. 1:24,000.
Folk, R.L. 1960. Petrography and origin of the Tuscarora, Rose Hill, and Keefer Formations, Lower and Middle Silurian of Eastern West Virginia. J. Sediment. Res. 30:1–58.
Gardner, T.W., J.B. Ritter, C.A. Shuman, J.C. Bell, K.C. Sasowsky, and N. Pinter. 1991. A periglacial stratified slope deposit in the valley and ridge province of central Pennsylvania, USA: Sedimentology, stratigraphy and geomorphic evolution. Permafrost Periglac. Processes 2:141–162.
Gillette, T. 1947. The Clinton of western and central New York. N.Y. State Mus. Bull. 341. New York State Museum, Albany, NY.
Godderis, Y., L.M. Francois, A. Probst, J. Schott, D. Moncoulon, D. Labat, and D. Viville. 2006. Modelling weathering processes at the catchment scale: The WITCH numerical model. Geochim. Cosmochim. Acta 70:1128–1147. doi:10.1016/j.gca.2005.11.018
Goodfellow, B.W., O.A. Chadwick, and G.E. Hilley. 2014. Depth and character of rock weathering across a basaltic-hosted climosequence on Hawai'i. Earth Surf. Processes Landforms 39:381–398. doi:10.1002/esp.3505
Harris, W., and G.N. White. 2008. X-ray diffraction techniques for soil mineral identification. In: A.L. Ulery and L.R. Drees, editors, Methods of soil analysis. Part 5. SSA Book Series 3. SSSA, Madison, WI.
Helgeson, H.C., R.M. Garrels, and F.T. MacKenzie. 1969. Evaluation of irreversible reactions in geochemical processes involving minerals and aqueous solutions—II. Applications. Geochim. Cosmochim. Acta 33:455–481. doi:10.1016/0016-7037(69)90127-6
Herndon, E.M., L. Jin, D.M. Andrews, D.M. Eissenstat, and S.L. Brantley. 2015. Importance of vegetation for manganese cycling in temperature forested watersheds. Global Biogeochem. Cycles 29:160–174. doi:10.1002/2014GB004858
Jackson, M.L. 1974. Soil chemical analysis—Advanced course. 2nd ed. Univ. of Wisconsin, Dep. of Soil Science, Madison.
Jenny, H. 1941. Factors of soil formation: A system of quantitative pedology. 1st ed. McGraw-Hill, Inc., New York.
Jin, L., R. Ravella, B. Ketchum, P. Heaney, and S.L. Brantley. 2010. Mineral weathering and elemental transport during hillslope evolution at the Susquehanna/Shale Hills Critical Zone Observatory. Geochim. Cosmochim. Acta 74:3669–3691. doi:10.1016/j.gca.2010.03.036
King, P.B., H.W. Ferguson, and W. Hamilton. 1960. Geology of northeasternmost Tennessee. U.S. Geol. Surv. Prof. Pap.:311. U.S. Gov. Print. Office, Washington, DC. 1:48,000.
Koch, G.W., P.M. Vitousek, W.L. Steffen, and B.H. Walker. 1995. Terrestrial transects for global change research. Vegetatio 121:53–65. doi:10.1007/BF00044672
Konert, M., and J. Vandenberghe. 1997. Comparison of laser grain size analysis with pipette and sieve analysis: A solution for the underestimation of the clay fraction. Sedimentol. 44:523–535. doi:10.1046/j.1365-3091.1997.d01-38.x
Kozak, S.J. 1965. Geology of the Millboro Quadrangle, Virginia. Virginia Div. Mineral. Resources Rep. Invest. 8. Virginia Division of Mineral Resources, Richmond, VA. 1:62, 500
Kump, L.R., S.L. Brantley, and M.A. Arthur. 2000. Chemical weathering, atmospheric CO_2, and climate. Annu. Rev. Earth Planet. Sci. 28:611–667. doi:10.1146/annurev.earth.28.1.611
Kunze, G.W., and J.B. Dixon. 1986. Pretreatment for mineralogical analysis. In: A. Klute, editor, Methods of soil analysis. Part I. SSSA, Madison, WI. p. 91–99.
Lebedeva, M.I., R.C. Fletcher, V.N. Balashov, and S.L. Brantley. 2007. A reactive diffusion model describing transformation of bedrock to saprolite. Chem. Geol. 244:624–645. doi:10.1016/j.chemgeo.2007.07.008
Lebedeva, M.I., R.C. Fletcher, and S.L. Brantley. 2010. A mathematical model for steady-state regolith production at constant erosion rate. Earth Surf. Processes Landforms 35:508–524.
Lybrand, R.A., and C. Rasmussen. 2015. Quantifying climate and landscape position controls on soil development in semiarid ecosystems. Soil Sci. Soc. Am. J. 79:104–116. doi:10.2136/sssaj2014.06.0242
Maher, K. 2010. The dependence of chemical weathering rates on fluid

residence time. Earth Planet. Sci. Lett. 294:101–110. doi:10.1016/j.epsl.2010.03.010

McKay, L.D., S.G. Driese, K.H. Smith, and M.J. Vepraskas. 2005. Hydrogeology and pedology of saprolite formed from sedimentary rock, eastern Tennessee, USA. Geoderma 126:27–45. doi:10.1016/j.geoderma.2004.11.017

Medlin, J.H., N.H. Suhr, and J.B. Bodkin. 1969. Atomic absorption analysis of silicates employing $LiBO_2$ fusion. Absorption Newsl. 8:25–29.

Minasny, B., A.B. McBratney, and S. Salvador-Blanes. 2008. Quantitative models for pedogenesis—A review. Geoderma 144:140–157. doi:10.1016/j.geoderma.2007.12.013

Mirabella, A., and M. Egli. 2003. Structural transformations of clay minerals in soils of a climosequence in an Italian alpine environment. Clays Clay Miner. 51:264–278. doi:10.1346/CCMN.2003.0510303

Moore, D.M., and R.C. Reynolds. 1997. X-ray diffraction and the identification and analysis of clay minerals. 2nd ed. Oxford Univ. Press, New York.

Muhs, D.R., E.A. Bettis, III, J. Been, and J.P. McGeehin. 2001. Impact of climate and parent material on chemical weathering in loess-derived soils of the Mississippi River Valley. Soil Sci. Soc. Am. J. 65:1761–1777. doi:10.2136/sssaj2001.1761

National Research Council. 2001. Basic opportunities in Earth Sciences. National Research Council, Washington, DC.

Poppe, L.J., V.F. Paskevich, J.C. Hathaway, and D. Blackwood. 2002. A laboratory manual for X-ray powder diffraction. U.S. Geological Survey Open File Rep. 01-041. U.S. Geological Survey, MA.

Rasmussen, C., S. Brantley, D.D. Richter, A. Blum, J. Dixon, and A.F. White. 2011. Strong climate and tectonic control on plagioclase weathering in granitic terrain. Earth Planet. Sci. Lett. 301:521–530. doi:10.1016/j.epsl.2010.11.037

Rasmussen, C., N.M. Matsuyama, R.A. Dahlgren, R.J. Southard, and N. Brauer. 2007. Soil genesis and mineral transformation across an environmental gradient on andesitic lahar. Soil Sci. Soc. Am. J. 71:225–237. doi:10.2136/sssaj2006.0100

Rasmussen, C., R.J. Southard, and W.R. Horwath. 2005. Modeling energy inputs to predict pedogenic environments using regional environmental databases. Soil Sci. Soc. Am. J. 69:1266–1274. doi:10.2136/sssaj2003.0283

Ruhe, R.V. 1984. Loess-derived soil of the Mississippi Valley region: II. Soil-climate system. Soil Sci. Soc. Am. J. 48:864–867. doi:10.2136/sssaj1984.03615995004800040033x

Runge, E.C.A. 1973. Soil development sequences and energy models. Soil Sci. 115:183–193. doi:10.1097/00010694-197303000-00003

Sanford, T.H. 1966. Generalized geologic map of Marshall County, Alabama. Map 60. Geological Survey of Alabama, Tuscaloosa, AL. 1:63,360.

Soil Survey Staff. 1993. National soil survey handbook. Title 430-VI. U.S. Gov. Print. Office, Washington, DC.

Soil Survey Staff. 2004. Soil survey laboratory methods manual. Soil Surv. Invest. Rep. 42. Version 4.0. USDA-NRCS, Washington, DC.

Stiles, C.A., C.I. Mora, and S.G. Driese. 2003. Pedogenic processes and domain boundaries in a Vertisol climosequence: Evidence from titanium and zirconium distribution and morphology. Geoderma 116:279–299. doi:10.1016/S0016-7061(03)00105-8

Strakhov, N.M. 1967. Principles of lithogenesis. Vol. 1. Oliver and Boyd Ltd., Edinburgh.

Taylor, G., and R.A. Eggleton. 2001. Regolith geology and geomorphology. J. Wiley & Sons, New York.

Tobish, O., and M. Turner. 1971. Geologic map of the San Sebastian Quadrangle, Puerto Rico. Puerto Rico: U.S. Geol. Survey Misc. Invest. Series Map I-661.U.S. Gov. Print. Office, Washington, DC.

Walter, R.C., and D.J. Merritts. 2008. Natural streams and the legacy of water-powered mills. Science 319:299–304. doi:10.1126/science.1151716

White, A.F., and S.L. Brantley. 1995. Chemical weathering rates of silicate minerals: An overview In: Chemical weathering rates of silicate minerals. Reviews in Mineralogy. Mineral. Soc. of Am., Washington, DC. p. 1–22.

White, A.F., M.S. Schulz, J.B. Lowenstern, D.V. Vivit, and T.D. Bullen. 2005. The ubiquitous nature of accessory calcite in granitoid rocks: Implications for weathering, solute evolution and petrogenesis. Geochim. Cosmochim. Acta 69:1455–1471. doi:10.1016/j.gca.2004.09.012

Whittig, L.D., and W.R. Allardice. 1986. X-ray diffraction techniques. In: A. Klute, editor, Methods of soil Analysis. Part 1. SSSA Book Ser. No. 9. ASA and SSSA, Madison, WI. p.331–362.

Williams, J.Z., J.Z. Bandstra, D. Pollard, and S.L. Brantley. 2010. The temperature dependence of feldspar dissolution determined using a coupled weathering-climate model for Holocene-aged loess soils. Geoderma 156:11–19. doi:10.1016/j.geoderma.2009.12.029

Williams, E.L., K. Szramek, L. Jin, T.C.W. Ku, and L.M. Walter. 2007. The carbonate system geochemistry of shallow groundwater/surface water systems in temperate glaciated watersheds (Michigan, USA): Significance of open system dolomite weathering. Geol. Soc. Am. Bull. 119:515–528. doi:10.1130/B25967.1

Wilson, M.J. 1999. The origin and formation of clay minerals in soils: Past, present and future perspectives. Clay Miner. 34:7–25. doi:10.1180/000985599545957

Wilson, M.J. 2004. Weathering of the primary rock-forming minerals: Processes, products and rates. Clay Miner. 39:233–266. doi:10.1180/0009855043930133

Yesavage, T., M.S. Fantle, J. Vervoort, R. Mathur, L. Jin, L.J. Liermann, and S.L. Brantley. 2012. Fe cycling in the Shale Hills Critical Zone Observatory, Pennsylvania: An analysis of biogeochemical weathering and Fe isotope fractionation. Geochim. Cosmochim. Acta 99:18–38. doi:10.1016/j.gca.2012.09.029